Palaeogeography, Palaeoclimatology, Palaeoecology 505 (2018) 398–409

Contents lists available at ScienceDirect

Palaeogeography, Palaeoclimatology, Palaeoecology

journal homepage: www.elsevier.com/locate/palaeo

Leukoma antiqua (Bivalvia) - A high-resolution marine paleoclimate archive for southern South America?

Samantha Rubo[a], Marina L. Aguirre[b], Sebastián M. Richiano[c], Rubén A. Medina[d], Bernd R. Schöne[a,*]

[a] Institute of Geosciences, University of Mainz, Johann-Joachim-Becher-Weg 21, 55128 Mainz, Germany
[b] CONICET and Facultad de Ciencias Naturales y Museo, Universidad Nacional de La Plata, Edificio Institutos, Laboratorios y Cátedras, calle 64 No 3, 1900 La Plata, Argentina
[c] Instituto Patagónico de Geología y Paleontología (CONICET–CENPAT), Boulevard Brown 2915, 9120 Puerto Madryn, Chubut, Argentina
[d] Universidad de Buenos Aires, Facultad de Ciencias Exactas y Naturales, Departamento de Ciencias Geologicas, Intendente Guiraldes 2160, Ciudad Universitaria, Buenos Aires, Argentina

ARTICLE INFO

Keywords:
Bivalve sclerochronology
Paleotemperature
Oxygen isotopes
Patagonian Sea
Disequilibrium

ABSTRACT

The Patagonian Sea in the SW Atlantic is one of the most productive marine ecosystems worldwide. Besides its economic relevance, this shelf sea serves as a major sink for atmospheric CO_2 and thus plays a major role in global climate. Despite that, the marine climate dynamics in that region remain barely known. Instrumental records only cover the last 30 years or so and high-resolution climate archives are currently not available. Here, we explore the possibility to obtain seasonally to inter-annually resolved paleotemperature data from shells of the bivalve mollusk, *Leukoma antiqua* collected alive from the shallow subtidal zone of the San Jorge Gulf. Results demonstrate that this species grows during summer and – at least at slow rate – during winter at this locality and records nearly the full seasonal temperature amplitude (monthly averages) in the form of $\delta^{18}O_{shell}$. Furthermore, isotope-based climate reconstructions will be limited to the first 15 years of life, because growth rates are sharply reduced afterward which aggravates sampling. The oldest studied specimen attained an age of 34 years. Annual, fortnightly and lunar daily increments can potentially be used to determine the timing and rate of seasonal shell growth and help placing the shell record into precise temporal context. However, due to interferences with the shell microstructure, sub-annual growth patterns were only occasionally well developed. In this study, the temporal alignment of the growth record was therefore largely achieved by forcing $T_{\delta 18O}$ to match the shape of the instrumental temperature curve. In some years it was possible to validate such temporal alignments with fortnight increments. Shell growth rate is strongly linked to primary production which attains a maximum in spring. For yet unexplained reasons, shell formation occurs with an offset of almost −1‰ (−0.9 ± 0.3‰) from expected oxygen isotopic equilibrium with the ambient water. When this offset is adjusted for, $\delta^{18}O_{shell}$ can be used to compute past water temperature. Given the individual variability regarding $\delta^{18}O_{shell}$, it is advised to study a sufficient number coeval specimens to obtain more reliable information on the seasonal temperature range. Presumably, the overall life history and the isotopic offset is similar for *L. antiqua* specimens at other localities in southern South America. Since *L. antiqua* not only dominates modern nearshore benthic assemblages, but also occurs abundantly in Quaternary deposits along the Argentine Patagonian coast, this species can significantly contribute to a better understanding of natural baseline conditions and past climate dynamics in southern South America.

1. Introduction

The Patagonian Sea in the SW Atlantic Ocean is one of the most productive marine ecosystems and one of the largest continental shelves (e.g., Longhurst et al., 1995; Carreto et al., 2007; Fernández et al., 2007; Dogliotti et al., 2014; Paparazzo et al., 2017; Fig. 1). Besides its economic relevance, this region serves as a major sink for atmospheric CO_2 with one of the highest uptake rates (Bianchi et al., 2005, 2009; Kahl et al., 2017; Orselli et al., 2018). Primary production in the Patagonian Sea is particularly strong near the numerous oceanic fronts at which water masses of different properties meet (Acha et al., 2004). From West to East, Carreto et al. (1995) distinguishes (1) the coastal

* Corresponding author.
E-mail address: schoeneb@uni-mainz.de (B.R. Schöne).

https://doi.org/10.1016/j.palaeo.2018.06.024
Received 3 April 2018; Received in revised form 12 June 2018; Accepted 13 June 2018
Available online 18 June 2018
0031-0182/

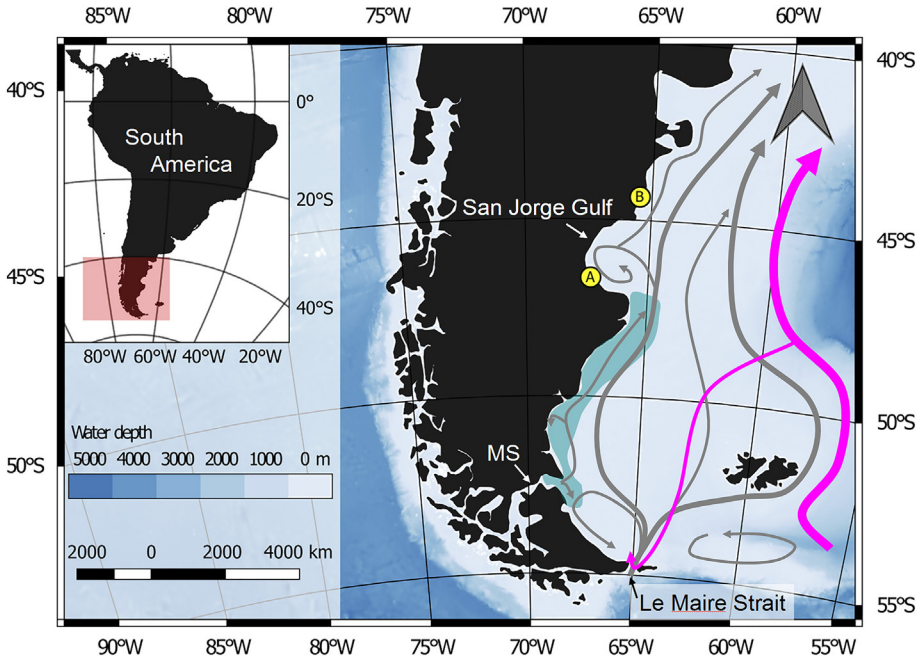

Fig. 1. Map showing localities at which living specimens of *Leukoma antiqua* were collected for the present study (A; sample ID = 2013-PAT3; see also Fig. 2) and for a previous study by Schellmann and Radtke (2007) (B). Major currents of the Patagonian shelf (grey) largely derive from the Cape Horn Current. The western boundary current (Malvinas/Falkland Current), a branch of the Antarctic Circumpolar Current, is depicted in purple. Waters from the latter flow as bottom currents (thin purple line) onto the Patagonian shelf and upwell through the Le Maire Strait. Fresher waters (Magellan Plume, green) deriving from the Magellan Strait (MS) are diluted as they move northward. At the southern tip of the San Jorge Gulf, the remainders of these waters are deflected offshore and can be traced up to ca. 42°S (references see Section 1). Origin of the map: gridded bathymetry data ("GEBCO 30 arc-second global grid of elevations") from the website www.gebco.net. Configuration of currents based on Matano et al. (2010). (For interpretation of the references to color in this figure legend, the reader is referred to the web version of this article.)

regime (comprising the upper 30 to 50 m) that is well mixed throughout the year by strong semidiurnal macrotides and westerly winds, (2) the tidal front, (3) the subantarctic shelf waters system which is stratified between spring and fall, and (4) the thermohaline shelf-break front that separates the shelf waters from the cooler, more saline and nutrient-rich Malvinas/Falkland Current (Kahl et al., 2017). Patagonian shelf waters mainly derive from the Cape Horn Current (Bianchi et al., 2005, Fig. 1), i.e., subantarctic waters that move around the southern tip of South America in eastward direction largely driven by the Westerlies. The West Wind Drift belt, in turn, is meridionally modulated by the Southern Annual Mode (also known as Antarctic Oscillation) which exhibits a statistically significant quasi-decadal variability of 8 to 16 years (Yuan and Yonekura, 2011). A poleward shift (= positive Southern Annual Mode) of the West Wind Drift belt results in increased poleward heat transport and increased kinetic energy of the ocean currents. In addition, deeper waters of the Malvinas Current upwell through the Le Maire Strait onto the Patagonian shelf and are then advected northward by westerly winds (Matano et al., 2010; Fig. 1). Relatively fresh waters enter the Patagonian Shelf from the Magellan Straits (Bogazzi et al., 2005; Lucas et al., 2005; Palma and Matano, 2012). The extension of the so-called Magellan Plume (Fig. 1) can be traced as far north as 42°S. However, near the southern tip of the San Jorge Gulf (ca. 47°S) the lower salinity waters are deflected offshore and separated from subantarctic waters by the Southern Patagonian Frontal System (Bogazzi et al., 2005). Therefore, the majority of the San Jorge Gulf (Fig. 1) and coastal areas further north are dominated today by subantarctic waters with a fairly stable salinity.

Knowledge of the complex oceanography of the Patagonian Shelf has benefitted a lot from remote sensing, direct measurements of water properties during research cruises, data collected at meteorological stations, and numerical simulations. However, the seasonal to interannual marine climate variability prior to the short instrumental era (30 years; Garreaud et al., 2013) remains largely unknown, because high-resolution marine proxy data are currently not available. Such data are required to constrain the natural baseline conditions, place ongoing changes in the area into a broader historical context and predict possible future changes. Shells of bivalves and gastropods can potentially provide respective paleoclimate data. However, only very few sclerochronological studies were conducted in southern South America, mainly along the coasts of Peru and Chile (Lazareth et al., 2006; Thébault et al., 2008; Gosselin et al., 2013) and the Beagle Channel (limpets: Colonese et al., 2012), but to our best knowledge only once on the Patagonian Shelf (Yan et al., 2012).

Here, we explore the possibility to obtain highly resolved temperature data from a combined analysis of shell growth patterns and stable oxygen isotope signatures of the shallow infaunal bivalve mollusk, *Leukoma antiqua* (King, 1832), previously assigned to the now-unaccepted genus *Protothaca*. *L. antiqua* not only dominates benthic faunal assemblages of modern nearshore (intertidal and shallow subtidal) environments in the Atlantic and Pacific Oceans (Carcelles, 1950; Carcelles and Williamson, 1951; Clasing et al., 1994; Rios, 1994; Urban and Tesch, 1996; Reid and Osorio, 2000); it also occurs abundantly in sedimentary strata along the Argentine Patagonian coast that formed during past warm intervals, in particular, the Mid-Holocene as well as MIS 5, 7, 9 and 11 (Feruglio, 1950; Aguirre, 2003; Aguirre et al., 2008, 2009, 2011; Schellmann and Radtke, 2007, 2010; Schellmann et al., 2008). In the present study, we conducted a detailed analysis of the timing and rate of shell formation of *L. antiqua* and investigated how faithfully the oxygen isotope data of its shell record changes of ambient water temperature. Through the use of multiple coeval specimens, we also addressed reproducibility aspects.

2. Material and methods

On 6 April 2013, several dozen specimens of *L. antiqua* were collected alive at low tide by apnea diving in ca. 3 m water depth in the shallow subtidal ESE of Caleta Olivia, Argentina (Golfo San Jorge; 46°29′23.10″S, 67°28′28.61″W; WGS84 datum; locality name: diving school "Cadace", Fig. 1). Bivalves were eviscerated immediately after collection and rinsed with seawater. At the same site, water samples were taken (in ca. 1 water depth) in 30 ml glass vials for the analysis of salinity (determined with a Schott handylab pH/LF12) and the stable oxygen isotope value of the water ($\delta^{18}O_{water}$) (Table 1).

2.1. Shell collection and preparation

Seventeen bivalves were arbitrarily chosen for subsequent analysis (Table 2). One valve of each specimen (again, arbitrarily left or right valves were chosen) was mounted on a Plexiglas cube with fast-curing plastic welder. To protect the shell during cutting, the inner and outer

Table 1
Stable oxygen isotope (average and 1 σ internal precision error) and salinity data of water samples collected in the study area.

Locality ID	Date	Locality	Lon/Lat	$\delta^{18}O_{water}$ (‰)	Salinity (PSU)
PAT3	26 January 2012	Cadace, Caleta Olivia	46°29′23.10″S, 67°28′28.61″W	−0.51 ± 0.08	
PAT3	12 March 2012	Cadace, Caleta Olivia	46°24′25.75″S, 67°20′40.44″W	−0.41 ± 0.06, −0.48 ± 0.07	
PAT3	6 April 2013	Cadace, Caleta Olivia	46°29′23.10″S, 67°28′28.61″W	−0.57 ± 0.03, −0.40 ± 0.02	33
PAT10	8 April 2013	Puerto Deseado	47°45′23.69″S, 65°53′27.95″W	−0.69 ± 0.04, −0.61 ± 0.03	32.6
PAT12	8 April 2013	Cañadon del Indio W Puerto Deseado	47°44′47.06″S, 65°58′9.71″W	−0.59 ± 0.03, −0.58 ± 0.03	32.9
PAT13	8 April 2013	Cañadon del Indio	47°44′31.60″S, 65°58′21.44″W	−0.08 ± 0.04, −0.12 ± 0.03	42.6
PAT14	9 April 2013	Rio Deseado at bridge	47°49′44.72″S, 66°35′36.50″W	−1.70 ± 0.05, −1.62 ± 0.02	0.5
PAT15	9 April 2013	Ensenada Ferrer	48°03′38.64″S, 65°57′38.92″W	−0.07 ± 0.08	33.1
PAT16	10 April 2013	Playa de los Caracoles	49°14′20.86″S, 67°40′02.73″W	−0.37 ± 0.06	32.5

The $\delta^{18}O_{water}$-salinity pairs were used along with selected GISS data to construct the regional freshwater mixing line (Fig. 2) except for values influenced by strong evaporation (PAT13 and PAT14). Coordinates are given in WGS datum.

Table 2
List of shells of *Leukoma antiqua* used in this study.

Specimen ID: 2013-PAT3-…	Ontogenetic age (yr)	# $\delta^{18}O_{shell}$	Purpose	$\delta^{18}O_{shell}$ (‰) at vm
A1L	5	24	so	
A2L	5	23	so	
A3L	10			
A4L	7	1	vm	−0.64 ± 0.05
A9L	8	18	so	
A13R	34	1	vm	−0.38 ± 0.04
A14L	5	26	so, vm	−0.86 ± 0.06
A15L	7	1	vm	−0.41 ± 0.06
A19R	8	25	so, vm	+0.30 ± 0.02
A20R	8	30	so	
A21L	10	29	so, vm	−0.81 ± 0.05
A26L	8	1	vm	−0.81 ± 0.05
A29R	27	1	vm	−0.69 ± 0.02
A33L	16	1	vm	−0.37 ± 0.03
A34L	6	40	so	
A35L	6	40	so	
A36L	12	1	vm	−0.68 ± 0.06

All specimens were collected alive on 6 April 2013. Column “Purpose” informs about the use of the isotope samples: so = identify seasonal oscillations, and determine timing and rate of shell growth as well as isotopic offset from expected equilibrium with seawater; vm = ventral margin samples (covering ca. last month of shell growth) were used as a second approach to determine the isotopic offset. $\delta^{18}O_{shell}$ averages and 1 σ internal precision errors are provided.

shell surface was covered with a ca. 1 cm broad stripe of epoxy resin along the axis of maximum growth. Along that axis, two ca. 2 to 3 mm-broad slabs were cut with a low-speed precision saw (Buehler Isomet 1000). These thick-sections were mounted on glass slides with epoxy resin, and the surface was ground with F800 and F1200 SiC grit powder on glass plates and then polished with 1 μm Al_2O_3 powder on a Buehler VerduTex cloth.

2.2. Growth pattern analysis

For growth pattern analysis, one polished cross-section was immersed in Mutvei's solution for 25 min (Schöne et al., 2005a). Stained sections were studied under a Wild Heerbrugg M8 stereomicroscope using sectoral dark field illumination (Schott VisiLED MC 1000; reflected light). Narrow growth patterns were investigated with a fluorescence light microscope (Zeiss AxioImager.A1m stereomicroscope, HBO 100 mercury lamp producing UV light, Zeiss filter set 18 with excitation and emission wavelengths of 390–420 nm (bandpass) and 450 nm (long pass), respectively; reflected light). Digital photographs were taken with a Canon EOS 600D camera. Growth increment widths (= distances between adjoining growth lines) were determined with an in-house image processing software, Panopea (Peinl and Schöne).

2.3. Sampling for stable isotopes of the shells

For the analysis of stable oxygen and carbon isotope values of the shells ($\delta^{18}O_{shell}$, $\delta^{13}C_{shell}$), a total of 255 powder samples were obtained from the outer sublayer of the outer shell layer (oOSL; ventral margin record; see Fig. 4A + B) of polished, unstained cross-sections of nine specimens (Table 2). In seven additional specimens, one sample was taken directly at the ventral margin to determine the isotopic composition of the last formed shell portion (Table 2). Note that in three of the nine other shells, one sample also covered the shell portion formed during ca. the last month of life.

According to XRD and Raman spectroscopic analyses of arbitrarily selected shell portions, the shells consisted entirely of aragonite; this information is relevant to choose the proper paleothermometry equation (see Section 2.4). Since the major goal of using stable isotope values was to determine whether the shells were precipitated in oxygen isotopic equilibrium with ambient water, only the last few (on average, five) years of growth were sampled. The ten so-called ‘ventral margin samples’ (see above) were used to double-check these results (Table 2).

In the majority of annual increments, shell carbonate powder was obtained by drilling holes in the oOSL with a conical SiC drill bit (300 μm diameter at the tip; Komet/Gebr. Brasseler GmbH & Co. KG, model no. H52 104 003). In slow-growing, ontogenetically older shell portions, high-resolution micromilling was applied to the last 3 to 5 mm near the ventral margin using a cylindrical, diamond-coated burr (1 mm diameter; model no. 835 104 010; for a graphic representation of the sampling technique see Fig. 12 in Schöne, 2008). Prior to sampling, the ventral margin was physically cleaned with abrasive paper or a dental burr to ensure that no contaminants were left. Then, shell powder was micromilled from the oOSL, guided by the shape of the growth lines. Each sample swath measured, on average, ca. 100 μm in width.

2.4. Stable isotope analysis

Stable oxygen isotopes of the water and shells were determined with a Thermo Fisher MAT 253 continuous-flow – isotope ratio mass spectrometer coupled to a GasBench II at the Institute of Geosciences, University of Mainz. For $\delta^{18}O_{water}$ analysis, water samples were processed using the equilibration method. For this purpose, 12 ml borosilicate exetainers were flushfilled with a mixture of 0.3 vol% CO_2 in He and loaded with 0.5 ml of water sample. Samples were equilibrated at 25 °C for 24 h. V-GISP2, V-SMOW2 and V-SLAP2 were used for calibration. Accuracy and average internal precision (Table 1) were better than 0.10‰ and 0.04‰, respectively.

Shell aragonite samples (39–120 μg, n = 293) were dissolved for 2 h in water-free phosphoric acid at 72 °C in He-flushed borosilicate exetainers. Data were calibrated against an in-house Carrara Marble standard ($\delta^{18}O = -1.91‰$; $\delta^{13}C = +2.01‰$). Accuracy (external precision) based on 421 blindly measured NBS-19 samples was better than 0.04‰ and 0.03‰, for $\delta^{18}O$ and $\delta^{13}C$, respectively. The average internal precision of the samples (computed from eight injections per

analysis) was better than 0.04‰ and 0.03‰, for $\delta^{18}O_{shell}$ and $\delta^{13}C_{shell}$, respectively. For stable carbon isotope data, the interested reader is referred to the Supplementary Data. Oxygen isotope values of the shells were not adjusted for differences in acid fractionation factors of aragonite (shells) and calcite (the Carrara Marble standard). For details see Füllenbach et al. (2015).

To reconstruct water temperatures from $\delta^{18}O_{shell}$ values, the paleothermometry equation by Grossman and Ku (1986) with a PDB-SMOW scale correction of −0.27‰ (Dettman et al., 1999) was employed.

$$T_{\delta^{18}O} = 20.34 - 4.34 \times (\delta^{18}O_{shell} - (\delta^{18}O_{water} - 0.27)) \quad (1)$$

For samples collected on 6 April 2013 at Cadace, we used the average $\delta^{18}O_{water}$ value measured at that time (−0.48‰). Potential temporal changes of the $\delta^{18}O_{water}$ signature were evaluated from seasonal and inter-annual salinity changes at the collection site and the regional freshwater mixing line. To determine the latter, water samples were also taken at several other localities and times along the Argentine Patagonian coast (Table 1). In addition, published $\delta^{18}O_{water}$ vs. salinity (S) pairs have been extracted from the NOAA Global Seawater Oxygen-18 Database (GISS data set, available at https://data.giss.nasa.gov/o18data/; last accessed on 4 October 2017; 54–70°W, 45–61.05°S, upper 35 m) and data reported by Daley et al. (2012) for precipitation in Puntas Arenas (Chile) and Ushuaia (Tierra del Fuego, Argentina) to further constrain the regional freshwater mixing line (Fig. 2). The respective equation is as follows.

$$\delta^{18}O_{water} = 0.2757 \times S - 9.65 \quad (2)$$

2.5. Instrumental data

Daily sea surface temperature (SST; Fig. 3) data were obtained from NOAA/ESRL/PSD from their webpage at www.esrl.noaa.gov (NOAA OI SST V2 High Resolution Dataset; 0.25° spatial resolution; center of data grid: 46°25′S, 67°25′W; Reynolds et al., 2007). Weekly resolved net primary production data (Fig. 3) data came from LP DAAC (AQUA/MODIS; 500 m spatial resolution) from their website at https://modis.ornl.gov/(center of data grid: 46°25′S, 67°25′W). Monthly resolved sea surface salinity data (UKMO dataset; 1° spatial resolution; center of data grid: 47°S, 67°W; Fig. 3) were downloaded from http://www.metoffice.gov.uk.

3. Results

3.1. Shell growth patterns

In the outer shell layer of polished and Mutvei-immersed cross-sections, major growth lines were observed (Fig. 4A–E), which compared well to such reported by Lazareth et al. (2006). In ontogenetically younger shell portions, these growth lines were often preceded by a succession of sub-annual bundles of growth lines that merged into a growth band which could easily be traced from the outer shell surface to the myostracum (Fig. 4A). However, during later years of life, the major growth lines became more and more distinct and were accompanied by a constriction on the outer shell surface (e.g., Fig. 4C + D). Some less distinct growth lines sometimes occurred ca. half-way between such major growth lines; but they could not easily be traced from the oOSL to the myostracum (see Fig. 4A). If the assumption holds true that the distinct lines formed on an annual basis as in many other bivalve species, studied specimens were between 5 and 34 years old (Table 2; Fig. 5). Note that the first (incomplete) annual increment at the umbo (= portion between the beak and the first annual growth line) was counted as year one, but the portion after the last annual increment was not considered as a year (see also Fig. 5).

The distance between these major growth lines (= annual growth increments) decreased exponentially (Figs. 4A and 5). At age 13 (2013-PAT3-A13L; Fig. 4B and E) or 15 (2013-PAT3-A29), the direction of shell growth changed abruptly by ca. 90° associated with a sharp decline of the growth rate. Instead of growing in height, the shells continued to grow in thickness by adding narrow, ca. 50 to 200 µm broad laminae forming a bulge at the ventral margin (Figs. 4B, E and 5).

In the oOSL of selected shell portions of a few specimens it was also possible to observe higher order growth patterns (Fig. 4F–H). Apparently, such shells were cut at an appropriate angle at which the shell microstructure (nondenticular composite prismatic) did not cover micrometer-scale growth patterns. Microgrowth increments reached widths of up to ca. 85 µm. About half way between adjacent microgrowth lines, a faint growth line was visible (Fig. 4G). Such growth patterns are often observed in intertidal bivalves exposed to semi-diurnal tides. Tentatively, these microgrowth patterns are thus referred

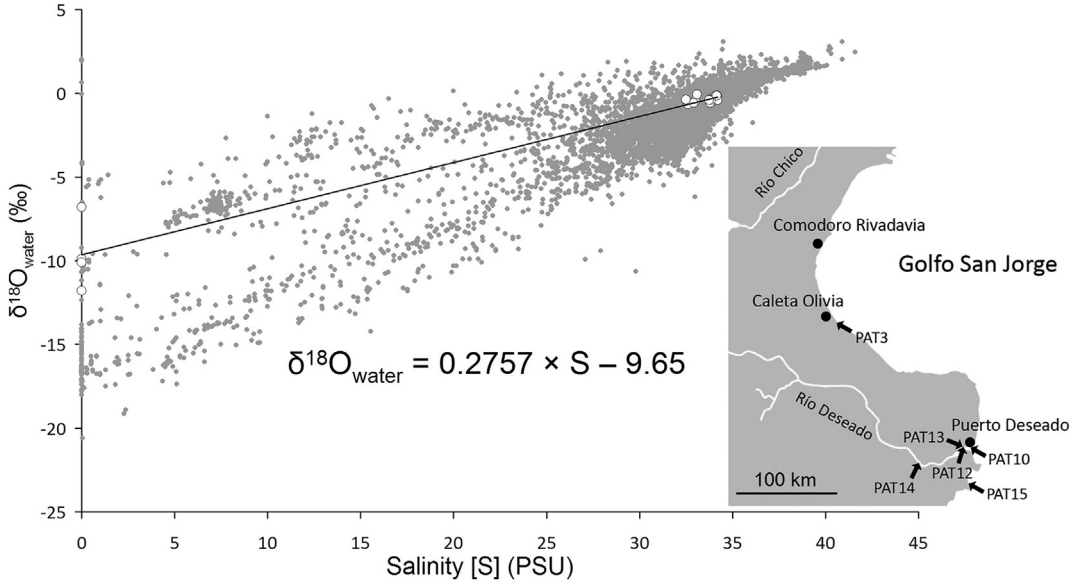

Fig. 2. Regional freshwater mixing line based on data (open circles) extracted from the GISS data set (spatial coverage: 45–61.05°S, 54–70°W, upper 35 m), water samples collected in this study (map with sample locality IDs; Table 1; excluding PAT13 and 14), and precipitation data reported in Daley et al. (2012). The remainder of the GISS data set (worldwide coverage) is depicted in grey for comparison.

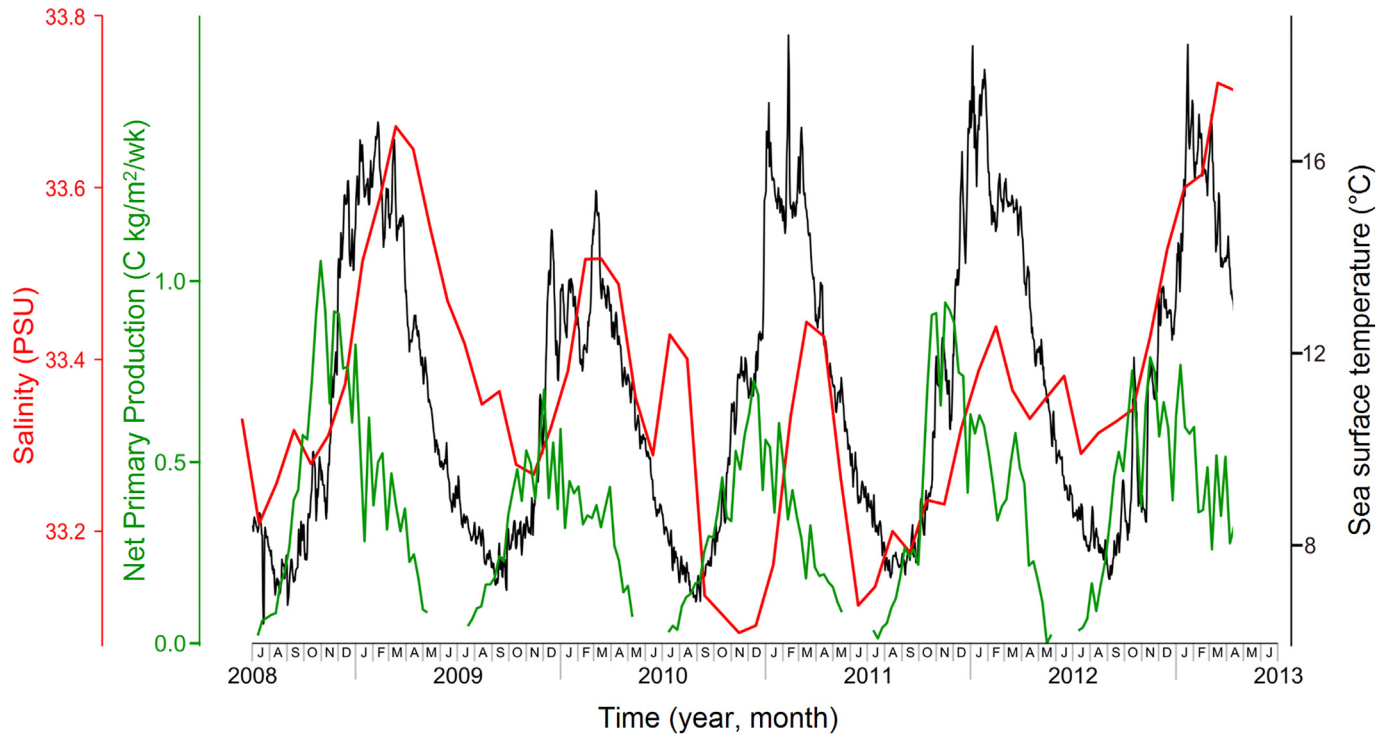

Fig. 3. Remotely sensed environmental data at the sample locality. The temporal resolution is daily for sea surface temperature (SST), weekly (wk) for net primary production and monthly for sea surface salinity. For details of the spatial coverages and data sources see Section 2.5.

to as 'lunar daily increments'. The lunar daily increments were arranged in bundles of alternating distinctness (Fig. 4F and H). Up to 22 of such bundles were visible within the second annual increment in few specimens. The number of microgrowth increments in these bundles, i.e., 14 to 15 (Fig. 4H), further supports the hypothesis that the microgrowth increments represent lunar days and the bundles represent fortnights. In general, the distance between the presumed fortnight bundles gradually increased from about 200 µm immediately after the major growth lines, abruptly reached a maximum of ca. 750 µm about 2/3 way after the growth line and then decreased sharply close to the following major growth line. For later comparison with daily instrumental temperature data, we have exemplarily computed the average (lunar) daily shell rate per fortnight cycle of the second year of growth of specimen 2013-PAT3-A1L (Fig. 6). For this purpose, each fortnight increment width was divided by 14.

3.2. Shell stable isotope data

Shell oxygen isotope profiles showed saw-tooth shaped variations with an amplitude of up to 1.88‰ (specimen 2013-PAT3-A2L; Fig. 7). Within one cycle and in the direction of growth, in the majority of sampled shells, $\delta^{18}O_{shell}$ values became gradually more negative, reached a minimum and then changed quickly to more positive values (Fig. 7). Major growth lines were typically located shortly after the most negative $\delta^{18}O_{shell}$ value of a cycle (Fig. 7) suggesting that these lines formed on a periodic basis in late summer/early fall. This assumption is further corroborated by the presence of a fully developed major growth line followed by a fraction of a new annual increment directly at the ventral margin of fast-growing, young individuals collected in early April (Fig. 4A, C and D). The timing of the growth line formation can therefore be narrowed down to approximately February/March. The $\delta^{18}O_{shell}$ values of powder samples taken from the last formed shell portion (representing ca. the last month prior to death) of ten specimens (Table 2) equaled, on average, −0.43 ± 0.40‰. The remaining 255 isotope samples, covering ca. the last five years, returned an average $\delta^{18}O_{shell}$ value of 0.17 ± 0.48‰ (1σ), and extreme values of −1.06‰ and 1.32‰.

3.3. Water temperature estimated from $\delta^{18}O_{shell}$ and temporal alignment of the growth record

At the time of collection (6 April 2013), the water at Cadace (locality ID 2013-PAT3) measured ca. 13 °C, had a salinity of ca. 33, and $\delta^{18}O_{water}$ value equaled, on average, −0.48 ± 0.16‰. This value is based on two separate measurements of the same water sample (Table 1). The propagated 1 σ error considers the accuracy of the mass spectrometer for $\delta^{18}O_{water}$ (± 0.10‰), the internal precision of the water measurements (± 0.03‰ and ± 0.02‰, respectively; Table 1), and the 1 σ variance of the mean of two measurements of the same water sample (± 0.12‰). Water samples taken at the same locality in January and March 2012 returned nearly identical values (Table 1). Furthermore, as indicated by remotely sensed data, between 2008–April 2013 (= shell portions deposited during that time interval were isotopically sampled in this study) salinity (and hence $\delta^{18}O_{water}$) fluctuated only in a very narrow range of 33.06 and 33.72 (arithmetic mean ± 1 σ = 33.35 ± 0.16) (Fig. 3). Using the regional freshwater mixing line (Fig. 2; Eq. (2)), this translates into an average $\delta^{18}O_{water}$ signature of −0.46 ± 0.04‰ and extreme values of −0.54 and −0.35‰. These data also compare well to the modeled long-term $\delta^{18}O_{water}$ value in the study area (LeGrande and Schmidt, 2006). To compute temperatures from the $\delta^{18}O_{shell}$ values of the samples collected at Cadace, we used the average $\delta^{18}O_{water}$ value measured on 6 April 2013 and include the 1 σ variance of the $\delta^{18}O_{water}$ values reconstructed from salinity data (0.04‰) in the propagated 1 σ error, hence −0.48 ± 0.17‰.

Using this $\delta^{18}O_{water}$ value and Eq. (1), the seasonal $\delta^{18}O_{shell}$ range of 1.88‰ (Section 3.2) translates into a temperature amplitude of 8.2 ± 0.7 °C (average ± 1 σ propagated error) which is nearly identical to the seasonal SST_{instr} range between 2008 and 2013, i.e., 7.8 ± 0.4 °C (average ± 1 σ error of the mean; based on monthly data). Since, on average, ca. eight isotope samples were taken per annual growth increment, comparison of $T_{\delta 18O}$ with monthly SST is thus

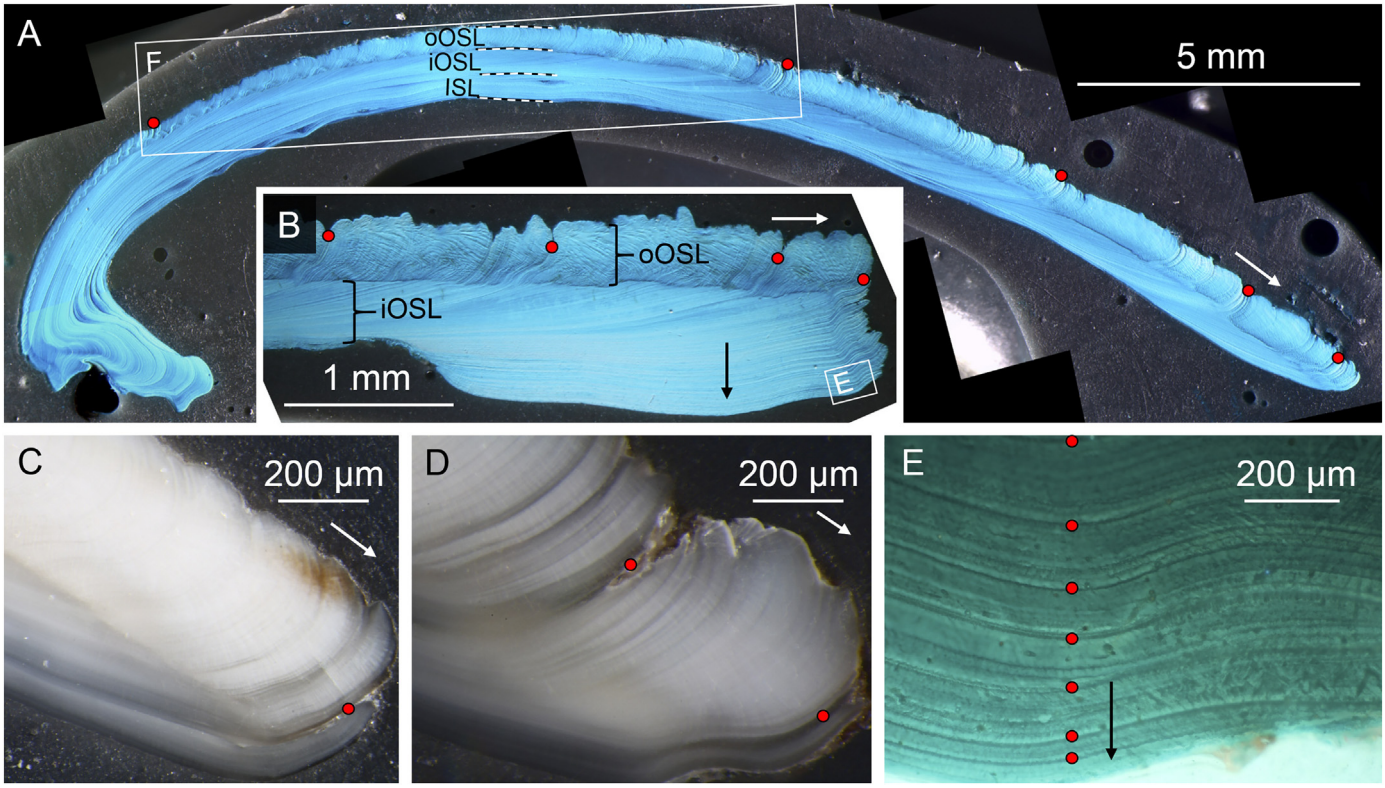

Fig. 4. Shell growth patterns of *Leukoma antiqua*. (A) Entire Mutvei-stained cross-section of specimen 2013-PAT3-A1L showing annual growth patterns. (B) Bulge at ventral margin of specimen 2013-PAT3-A13R (immersed in Mutvei solution) resulting from inward growth. Note abrupt change in direction of growth (from growth in height to growth in thickness). (C and D) At the time of collection on 6 April 2013, a fully developed annual growth line was present near the ventral margin and some percent of a new annual growth increment (2013) had already formed. Polished sections of specimen 2013-PAT3-A35L and 2013-PAT3-A34L, respectively. (E) Magnified portion of the ventral bulge of B. (F) Magnified portion of 2nd annual growth increment of specimen 2013-PAT3-A1L showing fortnightly growth patterns. (G) Lunar daily increments in specimen 2013-PAT3-A1L. Presumably, the more distinct growth lines (black solid line) were deposited during low tide at daytime and the faint lines (dashed) during low tide at night. (H) Fortnightly increments in an older shell portion of specimen 2013-PAT3-A13R. (A–F) reflected light, sectoral dark-field illumination. (G and H) Mutvei-immersed sections studied under UV light; see Section 2.2 for details. Red circles = annual growth lines. Yellow circles = fortnightly increments (spring tides). Arrows = direction of growth. oOSL, iOSL = outer, inner portion of the outer shell layer; ISL = inner shell layer. (For interpretation of the references to color in this figure legend, the reader is referred to the web version of this article.)

advised. Note that in Fig. 8, ca. monthly resolved $T_{\delta 18O}$ were plotted on top of the daily instrumental SST curve.

For the ten isotope samples from the ventral margin ($\delta^{18}O_{shell} = -0.53 \pm 0.39‰$; Table 2), we obtain a $T_{\delta 18O}$ value of 19.7 ± 1.7 °C (average ± 1 σ propagated error: all errors listed earlier in this section plus the precision errors of individual isotope measurements and the 1 σ variance of the mean of the ten isotope samples). The sampled shell portions presumably represent ca. the last month prior to collection during which the average remotely sensed SST was 14.5 ± 0.7 °C (average ± 1 σ error of the mean; based on daily SST). Hence, (ca. monthly) temperatures reconstructed from $\delta^{18}O_{shell}$ values at the ventral margin overestimated instrumental SST by 5.2 ± 1.7 °C (average ± 1 σ propagated error). Note that the isotope data contains one outlier. If this were removed, the $T_{\delta 18O}$ value would be 20.0 ± 1.1 °C ($\delta^{18}O_{shell} = -0.63 \pm 0.26‰$) and daily instrumental SST would be overestimated by 5.5 ± 1.1 °C.

Temperatures were then computed from the remaining $\delta^{18}O_{shell}$ values (= those obtained by serial sampling), and the shell record placed in temporal context (Fig. 8). To do so, the temperature proxy data ($T_{\delta 18O}$) were so arranged that the shape of the daily instrumental SST curve was best fitted. However, instrumental SST were consistently overestimated by $\delta^{18}O_{shell}$-derived water temperatures by 3.8 ± 1.4 °C (average ± 1 σ error of the mean). If shifted by this value, reconstructed temperatures of the studied specimens agreed very well with instrumental SST (Fig. 8). The majority of data points covered spring and summer, fewer data occurred during the second half of the year (Fig. 8).

Since the distance between the isotope samples is known (Fig. 7) and the date of each sample can be obtained from the temporally aligned $T_{\delta 18O}$ (Fig. 8), it is also possible to compute daily growth rates as an alternative approach to the microgrowth pattern analysis presented in Section 3.1 (Fig. 6). For this purpose, the distance between sample spots was divided by the number of days that elapsed between these sample spots. Exemplarily, Fig. 6 shows the reconstructed daily growth curve of several years of growth for specimen 2013-PAT3-A2L. Growth rates were slow (average daily increment width: 10–30 µm) between April and September, increased sharply for about two months (October and November, 65–85 µm/day) and then rapidly declined to values between 5 and 10 µm per day (Fig. 6).

4. Discussion

In the study area, the San Jorge Gulf, this species *L. antiqua* grows during summer and winter (Fig. 8) and can thus potentially provide information on nearly the full seasonal temperature amplitude (at least on the basis of monthly averages) and likely other environmental data. However, some limitations occur. Firstly, due to reduced growth rates in the cold season, sampling resolution needs to be sufficiently high in respective shell portions to capture lowest winter temperatures. Secondly, the temporal alignment of the seasonal shell growth record can be accomplished with fortnight increments, if the shells were cut properly and microstructures do not interfere with growth patterns.

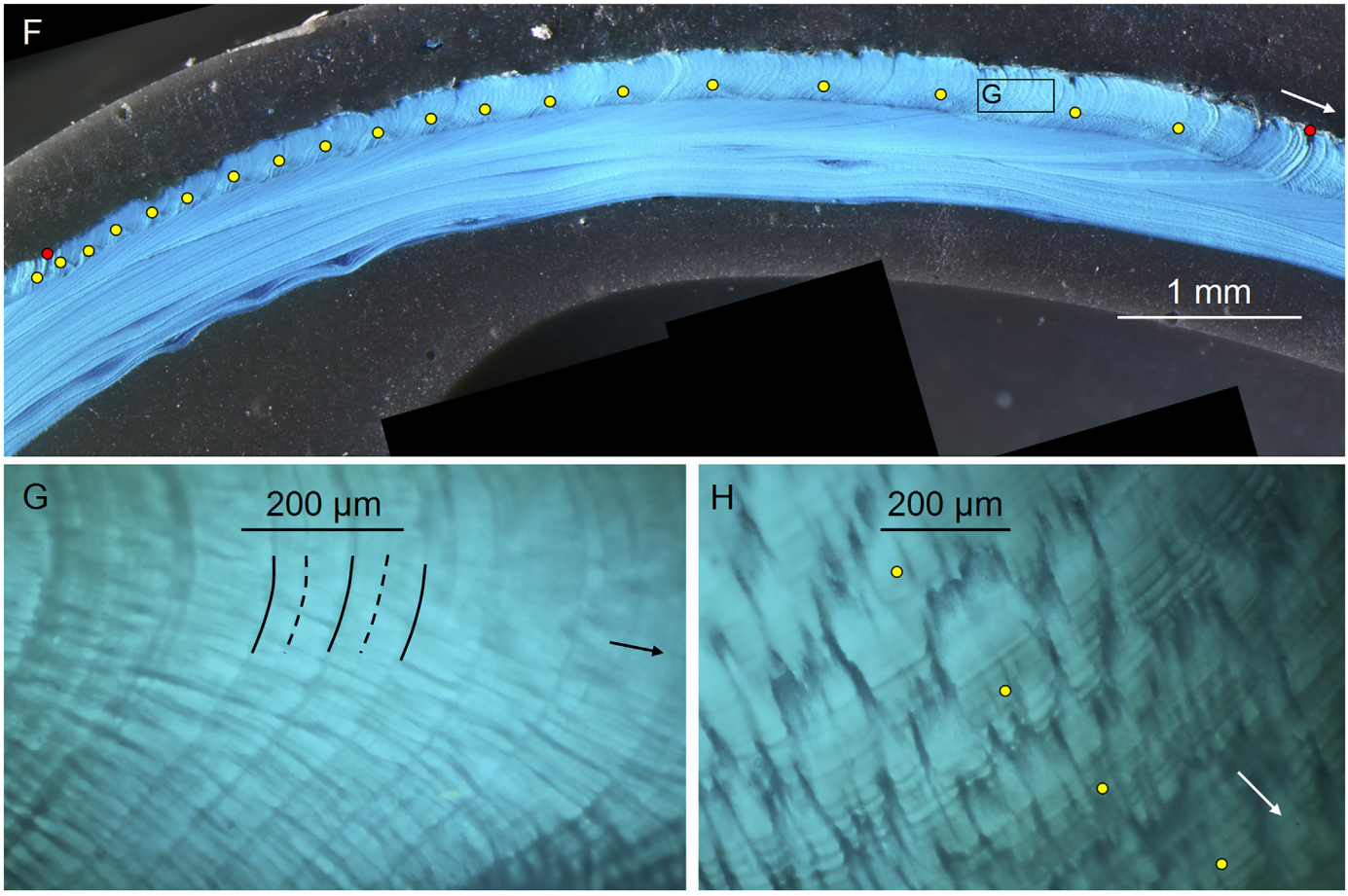

Fig. 4. (*continued*)

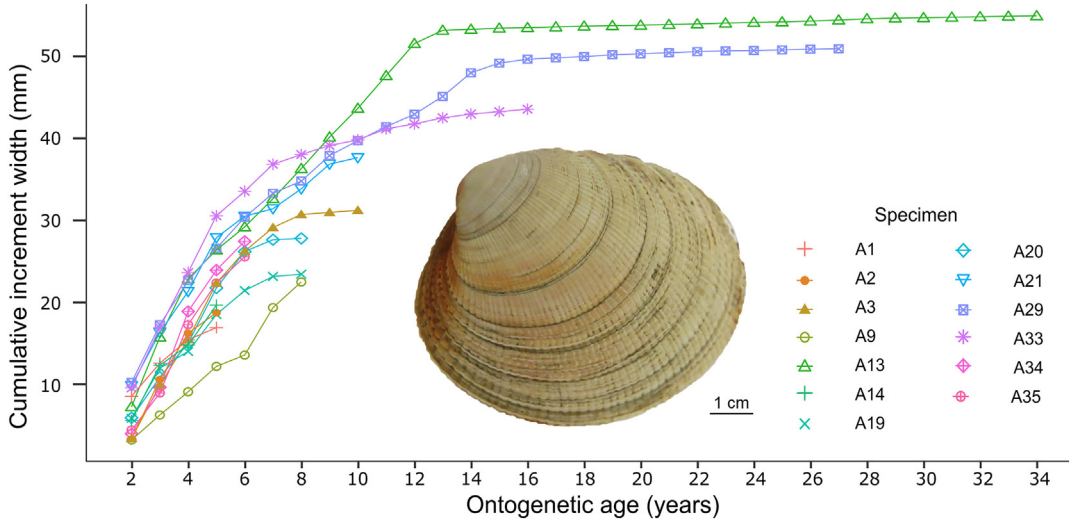

Fig. 5. Cumulative growth curves of *Leukoma antiqua*. Also shown is the left valve (outer shell surface) of specimen 2013-PAT3-A4.

Sub-annual increments are only occasionally well developed. Thirdly, isotope-based climate reconstructions will be limited to the first ca. 13 to 15 annual increments, because shell growth rate is sharply reduced afterward (Figs. 4B+E and 5; bulge at the ventral margin, compare Zolotarev, 1980) which greatly aggravates sampling. It is also not clear if the timing and rate of seasonal shell growth remains the same after this drop in growth rate and change in growth direction (from growth in length to growth in thickness). Lastly, in contrast to the overwhelming majority of other bivalves, this species does not form its shell in oxygen isotopic equilibrium with the ambient water, but with a negative offset of −0.9 ± 0.3‰. This deviation from expected equilibrium exhibits some variability among specimens (resulting in a 1 σ temperature error of ± 1.4 °C), but remains fairly constant through lifetime. Hence, with a sufficient number of specimens, this vital effect can be mathematically eliminated from the isotope record (Fig. 8) and paleotemperatures can be estimated from $\delta^{18}O_{shell}$ of fossil specimens of *L. antiqua*. The results of the present study (life history, isotopic offset) are likely not limited to *L. antiqua* specimens in the San Jorge Gulf, but

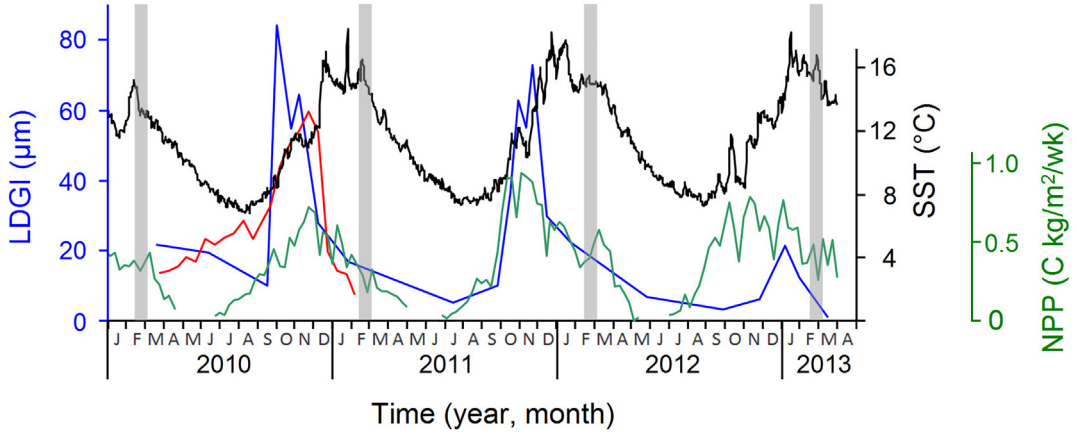

Fig. 6. Relation between lunar daily growth increment width (LDGI) of *Leukoma antiqua* and sea surface temperature (SST) and net primary production (NPP). SST and NPP as in Fig. 3. Average LDGI per fortnight was independently computed from time elapsed between sample spots for shell oxygen isotopes (see Section 3.3; blue curve; exemplarily, data from specimen 2013-PAT3-A1L are depicted; Fig. 8) and fortnightly increment widths (red curve; exemplarily, data from specimen 2013-PAT3-A2L are shown; Fig. 4F). Average LDGI per fortnight was computed from the time elapsed between sample spots for shell oxygen isotopes (blue curve; specimen 2013-PAT3-A1L; Fig. 8) and fortnightly increment widths (red curve; specimen 2013-PAT3-A2L; Fig. 4F). (For interpretation of the references to color in this figure legend, the reader is referred to the web version of this article.)

would certainly also be valid for other populations of this species in the Patagonian Sea and to fossil representatives of this species.

4.1. Oxygen isotopic disequilibrium in Leukoma

Multi-year temperature curves computed from $\delta^{18}O_{shell}$ values of *L. antiqua* overestimated instrumental temperatures by 3.8 °C. However, as indicated by the 1 σ error (± 1.4 °C) of the mean, the oxygen isotopic offset from expected equilibrium with the ambient water differed among specimens (Fig. 8). Microhabitat differences (i.e., changes in salinity, $\delta^{18}O_{water}$ etc.) can probably be excluded as an explanation, because the specimens were collected at the same site (well-mixed water column, relatively flat seabed) and within a limited area not exceeding ca. 25 m or so. The temporal alignment of the isotope data could have contributed to the variability. Since sub-annual growth patterns were challenging to study in this species, we have placed the shell record into temporal context by aligning the isotope-derived temperature data so that they matched the shape of the instrumental temperature curve. Where available, the fortnight growth patterns were used to validate this dating method, but in many annual increments, the sub-annual growth patterns were not visible and thus, we could not double-check the isotope-based dating method. Furthermore, it is possible that the isotopic offset is larger in some and smaller in other specimens, i.e., individual differences occur.

According to the ventral margin samples of ten specimens (Table 2), the isotopic offset was 1.4 °C larger than implied by the method above,

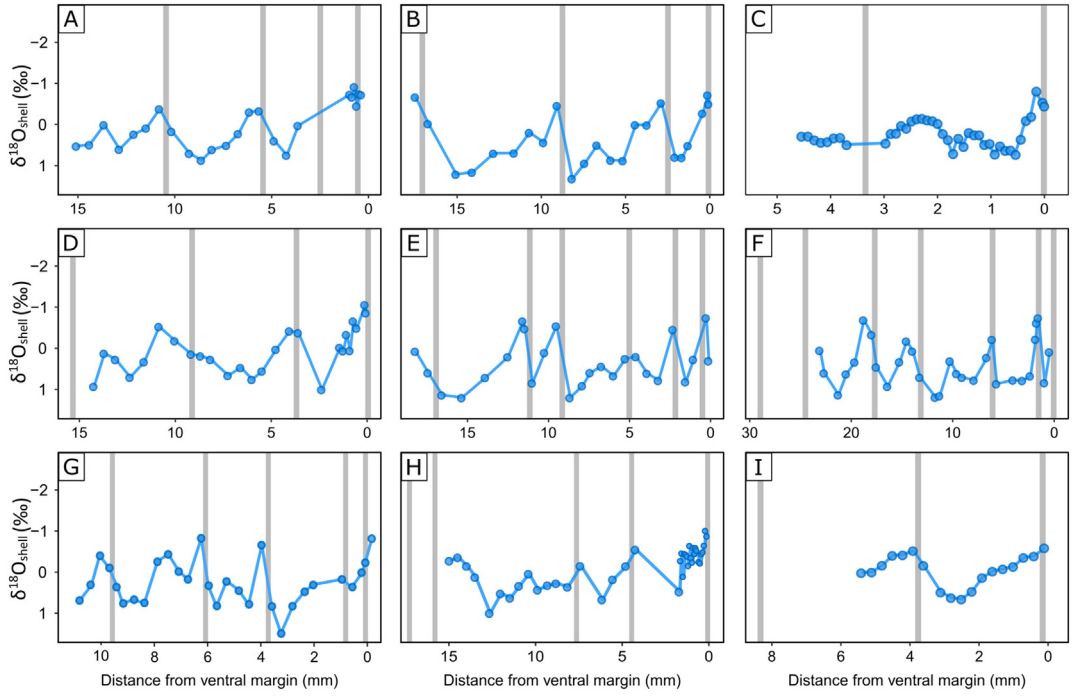

Fig. 7. Stable isotope data of *Leukoma antiqua*. Y-axes reversed to facilitate comparison with other figures. (A) Specimen 2013-PAT3-A1L, (B) A2L, (C) A9L, (D) A14L, (E) A19R, (F) A20R, (G) A21R, (H) A34L, (I) A35L. The propagated 1 σ error is ± 0.06‰. Higher density of data points near the ventral margin results from higher sampling resolution via milling instead of drilling. Direction of growth is to the right. Grey vertical bars denote annual growth lines.

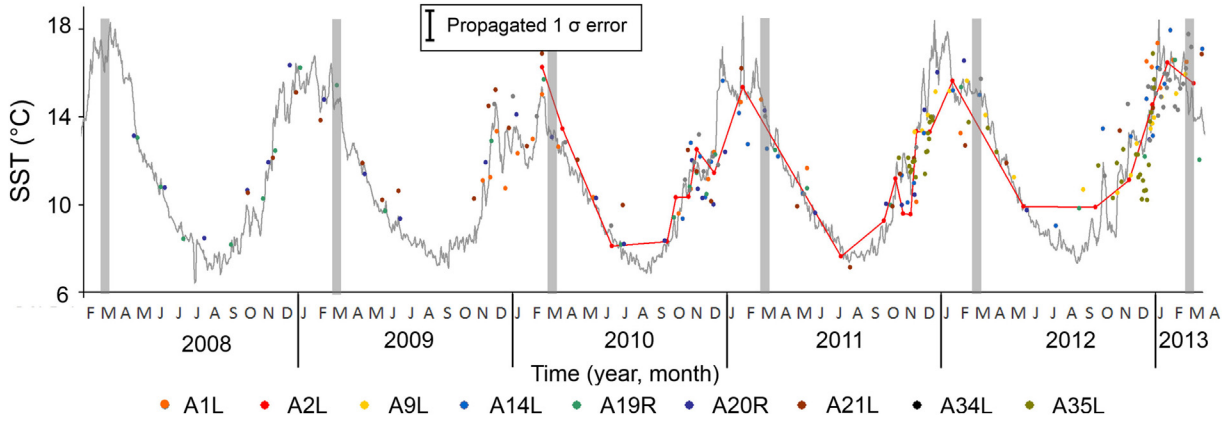

Fig. 8. Shell (of *Leukoma antiqua*) oxygen isotope-derived temperatures (shifted by −4 °C) and daily instrumental sea surface temperature (SST). Grey vertical bars denote annual growth lines. Exemplarily; $T_{\delta 18O}$ of specimen 2013-PAT3-A2L are linked by a line for better comparison with instrumental SST curve. The 1 σ error of the temperature estimates is ± 1.4 °C.

and likewise, the variance was higher, i.e., 5.2 ± 1.7 °C (and 5.5 ± 1.1 °C if the outlier were removed). Partly, this finding may be explained be the lower number of samples (10 vs. 255), and therefore, the offset value obtained by the multi-year method should be more reliable. The large variance supports the interpretation that individual differences exist regarding isotopic disequilibrium. In turn, the larger offset value may result from different time-averaging. In some specimens, the ventral margin samples may represent only a week or two of growth, but more than a month in others. Due to the lack of well-developed daily increments in these shell portions, we are unable to specify the time covered by these samples. Notably, during the last month prior to death, daily instrumental SST fluctuated by 0.7 °C, and this value further increases the more time is averaged.

Our study is not the first to report light stable isotope data of *L. antiqua* (see Schellmann and Radtke, 2007), but we have presented the first detailed sclerochronological calibration of this species and noticed a significant shell oxygen isotope disequilibrium with seawater. Schellmann and Radtke (2007) published oxygen isotope data of a *L. antiqua* specimen collected alive at Bahía Vera N Camarones, ca. 200 km north of Caleta Olivia (Fig. 1). The $\delta^{18}O_{shell}$ data given by these authors ranged from −0.70 to +1.44‰ (N = 80) which is close to the values obtained in the present study. Schellmann and Radtke (2007) used the distinct seasonal $\delta^{18}O_{shell}$ oscillations to estimate the ontogenetic age of the bivalve, but otherwise focused on the chronostratigraphy and geomorphology of the area. An interpretation of the stable isotope data and comparison with environmental data or a description of analytical details was therefore not provided. We can, however, compute temperatures from their $\delta^{18}O_{shell}$ data by considering the local $\delta^{18}O_{water}$ signature (−0.20 ± 0.06‰) at the study site of Schellmann and Radtke (2007) which, in turn, can be inferred from monthly resolved remotely sensed sea surface salinity records (34.28 ± 0.05; 1980–2007; center of grid: 44°16′S, 65°13′W) and the freshwater mixing line presented herein (Fig. 2; Eq. (2)). According to these calculations, $\delta^{18}O_{shell}$-derived temperatures ranged between 12.1 °C and 21.4 °C and overestimated monthly instrumental SST (7.8 to 17.3 °C) by 4.3 °C and 4.1 °C, respectively, resulting in an average temperature offset (4.2 °C) which is very near that identified in the present study (3.8 ± 1.4 °C).

A negative offset from expected oxygen isotopic equilibrium with seawater may be a common feature of the genus *Leukoma*. According to Lazareth et al. (2005, 2008), *L. thaca*, a close relative of *L. antiqua* from northern Chile and southern Peru likewise shows lower $\delta^{18}O_{shell}$ values than expected for equilibrium formation, and temperatures reconstructed thereof consistently overestimated actual water temperatures. These authors concluded that the shells were either not precipitated in oxygen isotopic equilibrium with the ambient water or the seawater isotopic composition exhibited unrecognized local variations. Note that the studies by Lazareth et al. (2005, 2008) were conference contributions and no detailed information on the actual isotopic offset was given.

For another close relative of *L. antiqua*, i.e., *L. staminea* from northern California, Takesue and van Geen (2004) suggested shell formation to occur in oxygen isotopic equilibrium. However, their interpretation is not based on robust environmental data. Indeed, the exact temperature and $\delta^{18}O_{water}$ value at the site where the shells lived was not available, but were merely inferred from salinity data. The study locality, an intertidal flat, exhibited considerable seasonal and inter-annual changes in salinity (25.8 to 36.7), and thus $\delta^{18}O_{water}$ values computed thereof (−2.7 to +0.8‰). A more detailed analysis would clearly be required to confirm their interpretation.

4.2. Oxygen isotopic offset in bivalves and possible explanations

The great majority of bivalves form their shells near oxygen isotopic equilibrium with the ambient water which is an important prerequisite for using bivalve shells as paleoclimate archives. In fact, the $\delta^{18}O_{shell}$ signal reproducibility among conspecific bivalves of the same population is often better than 0.2‰ (Gillikin et al., 2005). However, exceptions have been reported from several taxa (e.g., Thébault et al., 2007). In *Arctica islandica*, for example, the inner portion of the outer shell layer (iOSL) was found to be enriched in ^{18}O relative to equilibrium and have 0.3‰ higher $\delta^{18}O_{shell}$ values than contemporaneous shell portions of the oOSL (Trofimova et al., 2018) (which presumably is deposited in oxygen isotopic equilibrium). These differences were explained with physical and chemical differences of the two shell layers visually expressed by different microstructures (oOSL = homogenous; iOSL = crossed-acicular/crossed-lamellar microstructure). However, the observed oxygen isotopic offset in *L. antiqua* is negative and more than three times larger than in *A. islandica*, and the samples came exclusively from the oOSL (nondenticular composite prismatic microstructure; Carter, 1990).

A large negative offset (ca. −1‰) from expected thermodynamic equilibrium has previously been reported from *Panopea abrupta* from Washington State (Hallmann et al., 2008) and *Eurhomalea exalbida* from the Falkland Islands (Yan et al., 2012). Actual temperatures were overestimated by $\delta^{18}O_{shell}$ values of these bivalves by more than 3–4 °C. This discrepancy may at least partly be explained by the lifestyle of these bivalves and the specific environmental setting in which they lived. Both species belong to the deep infauna, live deeply buried in the sediment, and their soft body is exposed to pore water that presumably is enriched in ^{16}O due to submarine freshwater outflow. The shells of both species have likely been formed from a mixture of seawater

inhaled through the siphon and pore water that entered the body fluids through the mantle epithelium. If that is the case and the lower $\delta^{18}O_{water}$ signature of the mixture of waters is not be considered in the paleothermometry equation, the temperature reconstructed from $\delta^{18}O_{shell}$ values would return higher than actual values. Furthermore, both studies found an increasing negative offset from expected equilibrium with increasing ontogenetic age. This may reflect the increasing burial depth of the two species and the use of an increasing proportion of pore water to build the shell as they age.

For a variety of reasons, these explanations cannot be applied to *L. antiqua*. Ontogenetic $\delta^{18}O_{shell}$ trends were not observed in this species (Fig. 7), but the isotopic offset remained invariant (Fig. 8). Besides that, *L. antiqua* is a shallow infaunal bivalve that predominantly experiences well-mixed (strong winds and tides) surface water throughout lifetime. A significant change of the oxygen isotope signature of the surface water through precipitation or riverine influx is highly unlikely. Argentine Patagonia including the study area is very arid because evaporation and evapotranspiration rates are large (2000 mm per year; Torres et al., 2018) and precipitation rate very low (233 mm per year; Glembocki et al., 2015), and no major rivers enter the San Jorge Gulf.

Theoretically, submarine freshwater discharge could serve as an additional or alternative explanation for the observed isotopic offset in the shells. Based on Radium and Radon isotope data, Torres et al. (2018) showed that submarine freshwater discharge is a dominant feature of the Patagonian coasts of the Chubut and Santa Cruz provinces. Such freshwater flows to the sea can be several times higher than that of rivers (Kwon et al., 2014). It would hence be possible that the bivalves were exposed to water near the sediment-water interface with a lower $\delta^{18}O_{water}$ signature. On the other hand, one would expect seasonal and inter-annual variations in such submarine freshwater discharges which would have been reflected in variations of the $\delta^{18}O_{shell}$ offset. The $\delta^{18}O_{water}$ value of water samples from the fluffy layer and the pore water determined during different seasons and years would certainly shed more light on such aspects.

Kinetic effects can potentially also have resulted in disequilibrium fractionation, but this should have affected both measured isotope systems and resulted in a strong co-variance of $\delta^{18}O_{shell}$ and $\delta^{13}C_{shell}$. However, this is not the case here ($R = 0.41$, $R^2 = 0.17$; $\delta^{13}C_{shell}$ can be found in the Supplements). Thus, the oxygen isotopic disequilibrium in *L. antiqua* requires an alternative explanation. We suggest here that the hypothesis brought forward by Thébault et al. (2007) for *Comptopallium radula* and Yan et al. (2012) for *Eurhomalea exalbida* can also be applied to *L. antiqua* (and, perhaps, other bivalves with this kind of offset), i.e., a different pH in the extrapallial fluid than typically present in bivalves. For example, a higher pH value would favor the isotopically lighter carbonate ions over the isotopically heavier bicarbonate ions. An elevated pH at the site of shell formation could result from an enhanced Ca^{2+}-ATPase activity by which hydrogen ions are more effectively and faster removed through transmembrane pumps. To test this hypothesis, future studies should measure the pH in the extrapallial fluid.

4.3. Timing, rate and drivers of shell growth

Knowledge of the seasonal timing and rate of shell formation as well as the forcings of shell growth is an essential prerequisite prior to using bivalve shells for paleoclimate reconstructions. For example, an arithmetic mean of all $\delta^{18}O_{shell}$-derived temperature data from one 'annual' increment will typically not reflect the annual mean temperature, because barely any bivalve grows year-round and at the same rate (Schöne, 2008). It is therefore necessary to determine how fast the shell grew in each season and how much time is represented by each shell portion. Amongst others, this can be achieved through the analysis of periodic growth patterns.

Due to interferences with the shell microstructure, sub-annual growth patterns of the studied *L. antiqua* were only occasionally well developed (Fig. 4). None of the studied individuals showed distinct sub-annual growth patterns near the ventral margin, so that it remained impossible to directly test how much time is represented by these growth patterns. However, several clues suggest that the microgrowth patterns and their arrangement in bundles were controlled by the tides and represent lunar daily increments and fortnight increments, respectively. The alternating thick and thin microgrowth lines (Fig. 4) are typical features of intertidal bivalves exposed to semidiurnal tides (Ohno, 1989). The more distinct microgrowth lines are typically formed during high tides at daytime, whereas the faint microgrowth lines are deposited during high tides at night. During spring tides, the microgrowth lines are typically more distinctly developed than during neap tides (Hallmann et al., 2009). This should result in fortnightly bundles of microgrowth patterns of alternating distinctness as observed in the present study. The number of microgrowth increments within these recurring bundles as well as the number of bundles in an annual increment further supports the interpretation of tide-controlled growth patterns. Given the strong tides in the study region, it is not surprising to observe tide-controlled growth patterns even in bivalves living in the shallow subtidal zone.

In the present study, we estimated seasonal shell growth rates with two independent methods, i.e., by employing tide-controlled growth patterns and temporally aligned $\delta^{18}O_{shell}$ samples. Both methods revealed similar results (Fig. 6) according to which fastest shell growth occurred in austral spring (October and November), reduced growth during the austral winter months (April–July), and annual growth line formation between mid-February and mid-March, i.e., shortly after the seasonal temperature maximum. The findings are largely in agreement with two previous studies on *L. antiqua* from Chile based on mark-and-recovery experiments and monthly collections, respectively (Clasing et al., 1994; Stead et al., 1997). Previous studies further demonstrated that the genus *Leukoma* is highly tolerant to large temperature shifts (6° to 20 °C; Urban, 1994; Riascos et al., 2012) and, as in many other bivalves (Witbaard et al., 1997, Ansell, 1968 etc.), food availability is a major factor controlling growth (Riascos et al., 2012). Likewise our findings suggest a strong link between primary production and the timing and rate of shell growth of *L. antiqua*, because the majority of the annual increment was precipitated contemporaneously with the seasonal primary production maximum, and slower shell growth was largely associated with lower primary production (Fig. 6).

However, two observations require a different interpretation. Firstly, shell formation occurred even during times when no primary production was detected (May–June) (Figs. 6 and 8). We assume that the omnipresent strong vertical mixing of the water column by wind and tides (Acha et al., 2004; Matano et al., 2010; Palma and Matano, 2012) assured that suspended particulate organic matter was available as a food source at all times and represented the main energy source for the bivalves in the cold winter months. Alternatively, the bivalves may have used stored energy resources to continue shell formation while primary production ceased. Secondly, the formation of the annual growth line requires extremely slow and perhaps halted shell growth. It occurred at a time when primary production was still at a high level (Fig. 6). Scarcity of fresh food can thus be ruled out as a trigger for growth line formation. Interestingly, the annual growth line always formed shortly after the seasonal temperature maximum. Why *L. antiqua* forms annual growth lines at this time of the year remains difficult to understand. In some other species, spawning results in growth line formation (Sato, 1995; Purroy et al., 2018). However, in juvenile, likely premature specimens of *L. antiqua*, annual growth lines likewise formed during mid-February and mid-March. Furthermore, the main spawning period in this species occurs between November and February (Lozada and Bustos, 1984; Stead et al., 1997) or during winter (Riascos et al., 2012). We therefore suggest here that the annual growth line formation is causally linked to declining temperatures after the summer temperature maximum as previously reported for other species (e.g., Schöne et al., 2005b). Perhaps, the timing of annual growth line formation is genetically determined and maintained by internal biological

clocks that count the time that elapses after the seasonal temperature maximum to 'ensure' that growth ceases when specific, currently unknown environmental circumstances occur. At sub/tropical settings, *L. thaca* and *L. staminea* reportedly form annual growth lines in summer as a response to heat stress (Lazareth et al., 2005; Takesue and van Geen, 2004). More ecological research is clearly needed to identify the ultimate cause for annual growth line formation in this species.

5. Conclusions

As revealed by the findings herein, *Leukoma antiqua* can potentially serve as a high-resolution climate archive in the Patagonian Sea and provide information on the seasonal and inter-annual paleotemperature variability. It grows during summer and winter and thus records almost the full seasonal temperature amplitude (at least on the basis of monthly averages) provided that the sampling resolution is high enough, particularly in shell portions deposited during the cold season. Lunar daily and fortnightly growth patterns can best be observed in the second year of growth and used to construct a seasonal growth model that can be used to place the isotope data of each year into seasonal temporal context. In the present study, we have applied fortnight growth patterns to validate the oxygen isotope-based temporal alignment of the growth record. The majority of the annual increment forms in spring/early summer contemporaneously with maximum primary production. Shell formation is thus strongly positively coupled to the availability of fresh phytoplankton. Future work should investigate if changes in increment width can be used to assess past changes in primary production.

Shells of *L. antiqua* also grow at low rates in the dark, cold winter (May and June) although phytoplankton growth is near zero at that time. Presumably, the bivalves fall back on re-suspended organic matter that is available as a result of omnipresent strong winds and tides. Annual growth line formation representing extremely slow to halted growth takes place in February/March although primary production is still ongoing at moderate rates. Likely, declining temperatures after the summer maximum trigger the slowdown of shell growth. The ultimate reason for this remains unresolved and deserves further research.

The most peculiar finding is that the shells of *L. antiqua* are formed $-0.9 \pm 0.3‰$ away from expected equilibrium with the $\delta^{18}O_{water}$. Since this offset is fairly invariant through lifetime, it can be mathematically corrected for. Shell oxygen isotope-based paleotemperature estimates are hence feasible, and the amassing number of fossil (Quaternary) shells preserved along the coastal area or ancient beaches of the Patagonian Sea can be put at work. However, such studies should be based on more than one or two shells considering the oxygen isotopic variability ($\pm 0.3‰$) among coeval specimens.

Acknowledgments

We are greatly indebted to Alejandro Cortina for his help during sample acquisition and for borrowing us the diving equipment and to Juan Heupel for allowing us to work at Cadace. We also thank Michael Maus for his help during isotope analysis and keeping the mass spectrometer and peripheries in excellent shape. Furthermore, we thank Thomas M. Weber (formerly at Univ. Mainz) for helpful discussions and help during sample acquisition. We are grateful for very detailed and helpful comments provided by two anonymous reviewers which helped to improve the manuscript. This study was made possible by a research grant to MLA by DAAD-CONICET (DAAD: A/11/00682). Furthermore, BRS and MLA received a jointly funded grant by the Deutsche Forschungsgemeinschaft (SCHO 793/14) and CONICET. SR kindly acknowledges a stipend by the *Max Planck Graduate Center mit der Johannes-Gutenberg Universität Mainz*.

References

Acha, E.M., Mianzan, H.W., Guerrero, R.A., Favero, M., Bava, J., 2004. Marine fronts at the continental shelves of austral South America. Physical and ecological processes. J. Mar. Syst. 44, 83–105.

Aguirre, M.L., 2003. Late Pleistocene and Holocene palaeoenvironments in Golfo San Jorge, Patagonia: molluscan evidence. Mar. Geol. 194, 3–30.

Aguirre, M., Hlebzsebitch, J., Dellatorre, F., 2008. Late cenozoic invertebrate paleontology, with emphasis on mollusks. In: Rabassa, J. (Ed.), Late Cenozoic of Patagonia and Tierra del Fuego. Chapter 14, 285–326. Developments in Quaternary Science. 11 Elsevier.

Aguirre, M., Richiano, S., Álvarez, M.F., Eastoe, C., 2009. Malacofauna Cuaternaria del litoral Norte de Santa Cruz (Patagonia, Argentina). Geobios 42, 411–434.

Aguirre, M., Donato, M., Richiano, S., Farinati, E., 2011. Pleistocene and Holocene interglacial molluscan assemblages from Patagonian and Bonaerensian littoral (Argentina, SW Atlantic): palaeobiodiversity and palaeobiogeography. Palaeogeogr. Palaeoclimatol. Palaeoecol. 308, 277–292.

Ansell, A.D., 1968. The rate of growth of the hard clam *Mercenaria mercenaria* (L) throughout the geographical range. J. Cons. Perm. Int. Explor. Mer. 31, 364–409.

Bianchi, A.A., Bianucci, L., Piola, A.R., Pino, D.R., Schloss, I., Poisson, A., Balestrini, C.F., 2005. Vertical stratification and air-sea CO_2 fluxes in the Patagonian shelf. J. Geophys. Res. 110, C07003. http://dx.doi.org/10.1029/2004JC002488.

Bianchi, A.A., Pino, D.R., Perlender, H.G.I., Osiroff, A.P., Segura, V., Lutz, V., Clara, M.L., Balestrini, C.F., Piola, A.R., 2009. Annual balance and seasonal variability of sea-air CO_2 fluxes in the Patagonia Sea: Their relationship with fronts and chlorophyll distribution. J. Geophys. Res. 114, C03018. http://dx.doi.org/10.1029/2008JC004854.

Bogazzi, E., Baldoni, A., Rivas, A., Martos, P., Reta, R., Lobo Orensanz, J.M., Lasta, M., Dell'Arciprete, P., Werner, F., 2005. Spatial correspondence between areas of concentration of Patagonian scallop (*Zygochlamys patagonica*) and frontal systems in the southwestern Atlantic. Fish. Oceanogr. 14, 359–376.

Carcelles, A., 1950. Catálogo de los Moluscos Marinos de la Patagonia. In: Anales del Museo Nahuel Huapí. 2. pp. 41–100.

Carcelles, A., Williamson, S., 1951. Catálogo de los Moluscos Marinos de la Provincia Magallánica. In: Museo Argentino de Ciencias Naturales “Bernardino Rivadavia” Ciencias zoológicas. 2. pp. 225–383.

Carreto, J.I., Lutz, V.A., Carignan, M.O., Cucchi Colleoni, A.D., De Marcos, S.G., 1995. Hydrography and chlorophyll a in a transect from the coast to the shelf-break in the Argentinian Sea. Cont. Shelf Res. 15, 315–336.

Carreto, J.I., Carignan, M.O., Montoya, N.G., Cucchi Colleoni, D.A., 2007. Ecología del fitoplancton en los sistemas frontales del Mar Argentino. In: Carreto, J.I., Bremen, C. (Eds.), El Mar Argentino y sus Recursos Pesqueros 5. INIDEP, Mar del Plata, pp. 11–31.

Carter, J.G., 1990. Skeletal Biomineralization: Patterns, Processes and Evolutionary Trends. Volume II. Atlas and Index. Van Nostrand Reinhold, New York (101pp).

Clasing, E., Brey, T., Stead, R.A., Navarro, J.M., Asencio, G., 1994. Population dynamics of *Venus antiqua* (Bivalvia Veneracea) in the Bahía de Yaldad, Isla de Chiloé, Southern Chile. J. Exp. Mar. Biol. Ecol. 177, 171–186.

Colonese, A.C., Verdún-Castelló, E., Álvarez, M., Briz, I., Godino, I., Zurro, D., Salvatelli, L., 2012. Oxygen isotopic composition of limpet shells from the Beagle Channel: implications for seasonal studies in shell middens of Tierra del Fuego. J. Archaeol. Sci. 39, 1738–1748.

Daley, T.J., Mauquoy, D., Chambers, F.M., Street-Perrott, F.A., Hughes, P.D.M., Loader, N.J., Roland, T.P., van Bellen, S., Garcia-Meneses, P., Lewin, S., 2012. Investigating late Holocene variations in hydroclimate and the stable isotope composition of precipitation using southern South American peatlands: an hypothesis. Clim. Past 8, 1457–1471.

Dettman, D.L., Reische, A.K., Lohmann, K.C., 1999. Controls on the stable isotope composition of seasonal growth bands in aragonitic fresh-water bivalves (unionidae). Geochim. Cosmochim. Acta 63, 1049–1057.

Dogliotti, A.I., Lutz, V.A., Segura, V., 2014. Estimation of primary production in the southern Argentine continental shelf and shelf-break regions using field and remote sensing data. Remote Sens. Environ. 140, 497–508.

Fernández, M., Colleoni, D., Roux, A., Marcos, A., Fernández, E., 2007. Caracterización físico-química del sistema bentónico en el sector sur del Golfo San Jorge, Argentina. Rev. Biol. Mar. Oceanogr. 42, 177–192.

Feruglio, E., 1950. Descripción Geológica de la Patagonia. In: Dirección General de Yacimientos Petrolíferos Fiscales, Buenos Aires. Volume 3 (119 pp).

Füllenbach, C.S., Schöne, B.R., Mertz-Kraus, R., 2015. Strontium/lithium ratio in shells of *Cerastoderma edule* (Bivalvia) - A new potential temperature proxy for brackish environments. Chem. Geol. 417, 341–355.

Garreaud, R., Lopez, P., Minvielle, M., Rojas, M., 2013. Large-scale control on the Patagonian climate. J. Clim. 26, 215–230.

Gillikin, D.P., De Ridder, F., Ulens, H., Elskens, M., Keppens, E., Baeyens, W., Dehairs, F., 2005. Assessing the reproducibility and reliability of estuarine bivalve shells (*Saxidomus giganteus*) for sea surface temperature reconstruction: implications for paleoclimate studies. Palaeogeogr. Palaeoclimatol. Palaeoecol. 228, 70–85.

Glembocki, N.G., Williams, G.N., Góngora, M.E., Gagliardini, D.A., Lobo Orensanz, J.M., 2015. Synoptic oceanography of San Jorge Gulf (Argentina): A template for Patagonian red shrimp (*Pleoticus muelleri*) spatial dynamics. J. Sea Res. 95, 22–35.

Gosselin, M., Lazareth, C.E., Ortlieb, L., 2013. Sclerochronological studies in the Humboldt Current system, a highly variable ecosystem. J. Shellfish Res. 32, 867–882.

Grossman, E.L., Ku, T.-L., 1986. Oxygen and carbon isotope fractionation in biogenic aragonite: temperature effects. Chem. Geol. (Isot. Geosci. Sect.) 59, 59–74.

Hallmann, N., Schöne, B.R., Strom, A., Fiebig, J., 2008. An intractable climate archive - sclerochronological and shell oxygen isotope analyses of the Pacific geoduck, *Panopea*

abrupta (bivalve mollusk) from Protection Island (Washington State, USA). Palaeogeogr. Palaeoclimatol. Palaeoecol. 269, 115–126.
Hallmann, N., Burchell, M., Schöne, B.R., Irvine, G.V., Maxwell, D., 2009. High-resolution sclerochronological analysis of the bivalve mollusk *Saxidomus gigantea* from Alaska and British Columbia: techniques for revealing environmental archives and archaeological seasonality. J. Archaeol. Sci. 36, 2353–2364.
Kahl, L.C., Bianchi, A.A., Osiroff, A.P., Pino, D.R., Piola, A.R., 2017. Distribution of sea-air CO_2 fluxes in the Patagonian Sea: Seasonal, biological and thermal effects. Cont. Shelf Res. 143, 18–28.
Kwon, E.Y., Kim, G., Primeau, F., Moore, W.S., Cho, H.-M., DeVries, T., Sarmiento, J.L., Charette, M.A., Cho, Y.-K., 2014. Global estimate of submarine groundwater discharge based on an observationally constrained radium isotope model. Geophys. Res. Lett. 41. http://dx.doi.org/10.1002/2014GL061574.
Lazareth, C.E., LeCornec, F., Liétard, C., Lasne, G., Pierre, C., Ortlieb, L., 2005. Interpreting the microstructure and geochemical variations within *Protothaca thaca* (Mollusca, Bivalvia) shells of Chile and Peru. Geophys. Res. Abstr. 7, 10328.
Lazareth, C.E., Lasne, G., Ortlieb, L., 2006. Growth anomalies in *Protothaca thaca* (Mollusca, Veneridae) shells as markers of ENSO conditions. Clim. Res. 30, 263–269.
Lazareth, C.E., Liétard, C., Pierre, C., Ortlieb, L., 2008. Inter-individual and inter-site reproducibility of $\delta^{18}O$ profiles across *Protothaca thaca* (Bivalvia, Veneridae) shells from Peru and Chile. Geophys. Res. Abstr. 10 (EGU2008-A-06203).
LeGrande, A.N., Schmidt, G.A., 2006. Global gridded data set of the oxygen isotopic composition in seawater. Geophys. Res. Lett. 33, L12604. http://dx.doi.org/10.1029/2006GL026011.
Longhurst, A., Sathyendranath, S., Platt, T., Caverhill, C., 1995. An estimate of global primary production in the ocean from satellite radiometer data. J. Plankton Res. 17, 1245–1271.
Lozada, E., Bustos, H., 1984. Madurez sexual y fecundidad de *Venus antiqua antiqua* King & Broderip 1835 en la bahía de Ancud (Mollusca: Bivalvia: Veneridae). Rev. Biol. Mar. 20, 91–112.
Lucas, A., Guerrero, R., Mianzán, H., Acha, M., Lasta, C., 2005. Coastal oceanographic regimes of the Northern Argentine Continental Shelf (34–43°S). Estuar. Coast. Shelf Sci. 65, 405–420.
Palma, E.D., Matano, R.P., 2012. A numerical study of the Magellan Plume. J. Geophys. Res. 117, C05041. http://dx.doi.org/10.1029/2011JC007750.
Matano, R.P., Palma, E.D., Piola, A.R., 2010. The influence of the Brazil and Malvinas Currents on the Southwestern Atlantic Shelf circulation. Ocean Sci. 6, 983–995.
Ohno, T., 1989. Palaeotidal characteristics determined by micro-growth patterns in bivalves. Palaeontol. 32, 237–263.
Orselli, I.B.M., Kerr, R., Ito, R.G., Tavano, V.M., Mendes, C.R.B., Garcia, C.A.E., 2018. How fast is the Patagonian shelf-break acidifying? J. Mar. Syst. 178, 1–14.
Paparazzo, F., Williams, G., Pisoni, J., Solís, M., Esteves, J., Varela, D., 2017. Linking phytoplankton nitrogen uptake, macronutrients and chlorophyll-a in SW Atlantic waters: The case of the Gulf of San Jorge, Argentina. J. Mar. Syst. 172, 43–50.
Purroy, A., Milano, S., Peharda, M., Schöne, B.R., Thébault, J., 2018. Drivers of shell growth of the bivalve, *Callista chione* (L. 1758) – Combined environmental and biological factors. Mar. Environ. Res. 134, 138–149.
Reid, D., Osorio, C., 2000. The shallow-water marine Mollusca of the Estero Elefantes and Laguna San Rafael, southern Chile. Bull. Nat. Hist. Mus. London (Zool.) 66, 109–146.
Reynolds, R.W., Smith, T.M., Liu, C., Chelton, D.B., Casey, K.S., Schlax, M.G., 2007. Daily high-resolution-blended analyses for sea surface temperature. J. Clim. 20, 5473–5496.
Riascos, J.M., Avalos, C.M., Pacheco, A.S., Heilmayer, O., 2012. Testing stress responses of the bivalve *Protothaca thaca* to El Niño–La Niña thermal conditions. Mar. Biol. Res. 8, 654–661.
Rios, E., 1994. Seashells of Brazil, 2nd ed. Fundação Universidade do Rio Grande, Rio Grande (481 pp).
Sato, S., 1995. Spawning periodicity and shell microgrowth patterns of the venerid bivalve *Phacosoma japonicum* (Reeve, 1850). Veliger 38, 61–72.
Schellmann, G., Radtke, U., 2007. Neue Befunde zur Verbreitung und chronostratigraphischen Gliederung holozäner K üstenterrassen an der mittel- und südpatagonischen Atlantikküste (Argentinien) - Zeugnisse holozäner Meeresspiegelveränderungen. Bamberg. Geogr. Schr. 22, 1–91.
Schellmann, G., Radtke, U., 2010. Timing and magnitude of Holocene sea-level changes along the middle and south Patagonian Atlantic coast derived from beach ridge systems, littoral terraces and valley-mouth terraces. Earth-Sci. Rev. 103, 1–30.
Schellmann, G., Beerten, K., Radtke, U., 2008. Electron spin resonance (ESR) dating of Quaternary materials. Eiszeitalter Gegenwart Quat. Sci. J. 57, 150–178.
Schöne, B.R., 2008. The curse of physiology – Challenges and opportunities in the interpretation of geochemical data from mollusk shells. Geo-Mar. Lett. 28, 269–285.
Schöne, B.R., Dunca, E., Fiebig, J., Pfeiffer, M., 2005a. Mutvei's solution: an ideal agent for resolving microgrowth structures of biogenic carbonates. Palaeogeogr. Palaeoclimatol. Palaeoecol. 228, 149–166.
Schöne, B.R., Fiebig, J., Pfeiffer, M., Gleß, R., Hickson, J., Johnson, A.L.A., Dreyer, W., Oschmann, W., 2005b. Climate records from a bivalved Methuselah (*Arctica islandica*, Mollusca; Iceland). Palaeogeogr. Palaeoclimatol. Palaeoecol. 228, 130–148.
Stead, R.A., Clasing, E., Navarro, J.M., Asencio, G., 1997. Reproductive cycle and cohort formation of *Venus antiqua* (Bivalvia: Veneridae) in the intertidal zone of southern Chile. Rev. Chil. Hist. Nat. 70, 181–190.
Takesue, R., van Geen, A., 2004. Mg/Ca, Sr/Ca, and stable isotopes in modern and Holocene *Protothaca staminea* shells from a northern California coastal upwelling region. Geochim. Cosmochim. Acta 68, 3845–3861.
Thébault, J., Chauvaud, L., Clavier, J., Guarini, J., Dunbar, R.B., Fichez, R., Mucciarone, D.A., Morize, E., 2007. Reconstruction of seasonal temperature variability in the tropical Pacific Ocean from the shell of the scallop, *Comptopallium radula*. Geochim. Cosmochim. Acta 71, 918–928.
Thébault, J., Thouzeau, G., Chauvaud, L., Cantillánez, M., Avendaño, M., 2008. Growth of *Argopecten purpuratus* (Mollusca: Bivalvia) on a natural bank in Northern Chile: sclerochronological record and environmental controls. Aquat. Living Resour. 21, 45–55.
Torres, A.I., Andrade, C.F., Moore, W.S., Falechini, M., Esteves, J.L., Niencheski, L.F.H., Depetris, P.J., 2018. Ra and Rn isotopes as natural tracers of submarine groundwater discharge in the patagonian coastal zone (Argentina): an initial assessment. Environ. Earth Sci. 77. http://dx.doi.org/10.1007/s12665-018-7308-7.
Trofimova, T., Milano, S., Andersson, C., Bonitz, F., Schöne, B.R., 2018. Oxygen isotope composition of *Arctica islandica* aragonite in the context of shell architectural organization - implication for paleoclimate reconstructions. Geochem. Geophys. Geosyst. 19. http://dx.doi.org/10.1002/2017GC007239.
Urban, H.-J., 1994. Upper temperature tolerance of ten bivalve species off Peru and Chile related to El Niño. Mar. Ecol. Prog. Ser. 107, 139–145.
Urban, H.-J., Tesch, C., 1996. Aspects of the population dynamics of six bivalve species from southern Chile: Results of the 'Victor Hensen' cruise to the Magellan Strait and the Beagle Channel in October/November 1994. Arch. Fish. Mar. Res. 44, 243–256.
Witbaard, R., Duineveld, G.C.A., deWilde, P.A.W.J., 1997. A long-term growth record derived from *Arctica islandica* (Mollusca, Bivalvia) from the Fladen Ground (northern North Sea). J. Mar. Biol. Assoc. UK 77, 801–816.
Yan, L., Schöne, B.R., Arkhipkin, A., 2012. *Eurhomalea exalbida* (Bivalvia): a faithful recorder of climate in southern South America? Palaeogeogr. Palaeoclimatol. Palaeoecol. 250-252, 91–100.
Yuan, X., Yonekura, E., 2011. Decadal variability in the Southern Hemisphere. J. Geophys. Res. 116, D19115. http://dx.doi.org/10.1029/2011JD015673.
Zolotarev, V.N., 1980. The life span of bivalves from the Sea of Japan and Sea of Okhotsk. Sov. J. Mar. Biol. 6, 301–308.